Strathprints Institutional Repository

Mylonas, Dimitrios and Turkmen, Serkan and Khorasanchi, Mahdi (2013) *Numerical study of asymmetric keel hydrodynamic performance through advanced CFD.* In: Third International Conference On Innovation In High Performance Sailing Yachts, 2013-06-26 - 2013-06-28, Lorient.

http://strathprints.strath.ac.uk/

NUMERICAL STUDY OF ASYMMETRIC KEEL HYDRODYNAMIC PERFORMANCE THROUGH ADVANCED CFD

D. Mylonas, S. Turkmen and **M. Khorasanchi,** University of Strathclyde, Glasgow, UK
dimitri.mylonas@gmail.com, serkan.turkmen@strath.ac.uk, mahdi.khorasanchi@strath.ac.uk

The hydrodynamics of an asymmetric IACC yacht keel at angle of yaw are presented using simulations performed by advanced computational fluid dynamics using state-of-the-art software. The aim of the paper is to continue working on the improvement of numerical viscous flow predictions for high-performance yachts using Large Eddy Simulation and Detached Eddy Simulation on unstructured grids. Quantitative comparisons of global forces acting on the keel and wake survey are carried out. Qualitative comparisons include flow visualisation, unsteady and separated flow and other features. Star-CCM+ and the trimmed cell method give better forces and wake prediction compared to the unstructured mesh of ANSYS Fluent. Both solvers give good flow visualisation near and far field of the keel.

1 INTRODUCTION

Recent shift and progress in numerical and computational methods based on Computational Fluid Dynamics (CFD) has focused on aerodynamic applications of sails performance, due to the prominent arrival of the state-of-the-art catamarans ready to compete in the forthcoming America's Cup.

Free-surface hydrodynamics are also increasingly studied, partly due to the boost in computational resources and partly because of their importance in competitive sailing concerning flow interactions between appendages and hull in certain sailing conditions (e.g. Volvo Ocean Race).

Below the waterline, another area where CFD simulations play a crucial role is the design and performance of the appendages. Keel hydrodynamics are studied to gain an understanding of effects and interactions occurring in the near and far field flow, depending on the sailing conditions.

Keel, bulb, winglets and rudder should be developed accordingly in order to guarantee global optimal performances. The advantage of the numerical approach relies on the possibility to test several different configurations and to have a complete picture of the flow behaviour at every time instant.

The viscous hydrodynamic flow around a keel is important for several reasons:

- The transition from laminar to turbulent flow is still a delicate topic in numerical simulation that requires continuous investigation.
- The unsteady & separated flow is also a critical aspect that researchers want to grasp to minimise losses and constraints during races.
- Modelling the flow at key locations such as root-junction of keel, bulb and winglets helps predicting when they occur.
- The continuous need for validation of quantitative results for CFD codes is important for high

Reynolds number flow. Additionally, qualitative data that can provide practical help to those involved in yachting is necessary.

Information about local and global distribution of flow quantities (e.g. pressure, velocities, vorticity and turbulence) can be useful to improve the hydrodynamic performances of keels. Creating and computing the flow around the appendages can help understanding the formation of the main flow characteristics and their interaction with the boat components.

In this context, CFD simulations of keel hydrodynamics have been carried out in various published studies using numerical methods based on potential flow codes and Navier-Stokes solvers with varying level of quantitative success but with useful qualitative applications.

Ticono et al. [1] showed good agreement between wind tunnel tests of generic keels for the 1992 America's Cup campaign and potential flow/boundary layer computations validated against wind-tunnel data. Their findings concluded that the numerical method was suited for induced drag computations of the keel configurations, but lacked in accuracy in the predictions of the viscous resistance of the bulbs.

Werner et al. [2, 3] validated a potential flow code (SHIPFLOW) coupled with a boundary layer code against the wind tunnel tests on an America's Cup keel. The errors in the potential flow code coupled to the boundary layer solution results were within the experimental uncertainty (2% error for both lift and drag), but given that the correct panelisation is used (in some cases, absolute error was as high as 18%).

In addition, the same research group also performed RANS based calculations with comparisons in terms of lift, drag forces, and wake survey. The multi-block structured approach used grids ranging from 1 million to 2.6 millions cells; the finest mesh was adding up to 3.6 million. The errors of the RANS code (FLUENT) were found to be a little higher than the experimental uncertainty. The study reported that errors between the measured values and the RANS computations for a

wingless keel yielded differences of between 0.4% and 3% for lift, depending on the turbulence model, and between 0.3% and 12% for drag. For a winged-keel, the corresponding discrepancies were around 3% for both forces.

Ambrogi et al. [4] performed a RANS simulation of the flow field around the same keel using a viscous code developed by INSEAN. The study showed differences in terms of pressure contours, velocity fields, vorticity and comparisons with experiments in terms of non-dimensional global forces and axial velocity. An overgrid, structured mesh of 7 million cells was used. The authors reported quite large errors between numerical results and measured values, of the order of about 8% in drag and as much as 23% in lift, for both arrangements tested. The differences were put down as modelling errors.

Thys [5] used Werner's geometry to test and evaluate the non-viscous, potential flow CFD code RAPID .One configuration was tested (winglets in aft position). Forces were found to be within the uncertainty region of the experimental measurements; drag was over predicted, lift was good for one case, but bad for the other. Out of the three lift-prediction methods used, (pressure integration, Trefftz-plane method and wing theory) the first was found to be the most accurate.

Mylonas and Sayer [6] presented initial work based on the use of Large Eddy Simulation (LES) and Detached Eddy Simulation (DES) using a commercial CFD code with mixed success. Error in forces prediction was found to be high at times, depending on the model used and the mesh size, but qualitative observations were found to be useful and relevant to keel flow hydrodynamics.

The main motivation behind this research is to continue on the improvement of previous numerical study on advanced CFD using a LES and DES approach of keel hydrodynamic prediction.

In the present study, the hydrodynamics of an asymmetric IACC keel in idealised upwind conditions are simulated using advanced computational methods based on the LES and DES turbulence models inside a virtual wind tunnel. The problem is further defined in the next section, followed by an outline of the mathematical formulation and numerical solution. Finally, the results are presented and discussed, and include quantitative & qualitative comparisons between CFD models.

2 PROBLEM DESCRIPTION

The wind tunnel experiments by Werner et al [2] are used as a validation case for the numerical study presented here. The fully appended IACC model keel is placed in the test section of the wind tunnel where flow is simulated. The fin and the winglets have a NACA 0012 profile. The bulb has a flat bottom and a beaver tail tip. This is known to produce minimum drag, by extending the effective span of the keel and ensuring that the wetted area is not increased excessively. The dimensions of the keel are given in Table 1. The tunnel blockage ratio between the model frontal area and the section area was found to be around 3%, and does not exceed the recommended 7.5% limit; hence, it is neglected in the study. Several configurations were tested and a selection of results is presented in the paper.

Table 1: model keel dimensions in metres

Bulb Chord	1.365
Bulb Max Thickness	0.176
Fin Mean Chord	0.216
Fin Max Thickness, Mean Chord	0.026
Fin Span	0.613
Winglet Mean Chord	0.077
Winglet Max Thickness, Mean Chord	0.009
Winglet Span	0.252
Winglet Dihedral (deg)	17°
Winglet Pitch (deg)	0°

The asymmetry of the case is represented by an angle of attack between the undistorted inlet flow and the model. Constraints in the experimental wind tunnel set-up of the keel led to a yaw angle fixed around 4 degrees. Moreover, it can be observed that the fin is not perfectly aligned with the bulb, causing a further gap (Figure 1). This incurs flow separation at the trailing edge of the fin keel and aft part of the bulb, which will be investigated. In addition, this means that any computational model will have to be meshed entirely, instead of using a half-model, which is common norm in CFD when dealing with symmetric bodies.
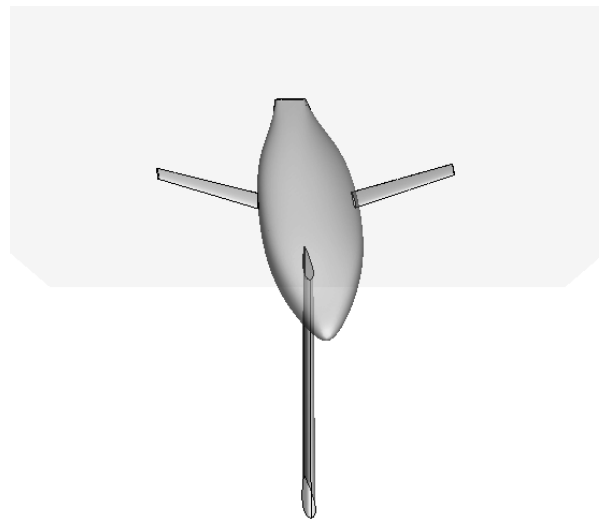

Figure 1: front view of the keel with yaw angle

The experiments reported the global forces in the undisturbed flow direction along the x-axis and the z-axis, corresponding to total drag and total lift forces. In addition to the forces, the following values were provided in the experimental data and were measured at a plane located at 2.375m from the tunnel inlet zone: velocity magnitude, velocity components in x-, y- and z- direction, static and total pressure. The inlet flow conditions are summarised in Table 2. The Reynolds number based on the length of the bulb and the free stream inlet velocity is equal to 3.2 x 10⁶, turbulent flow is expected around the keel.

Table 2: inlet flow conditions for CFD simulations

Atmospheric Pressure (kPa)	100.9
Inlet Velocity U_∞ (m/s)	36.27
Dynamic Viscosity μ (kg/ms)	$1.84 \cdot 10^{-5}$
Turbulent Intensity (%)	0.1
Turbulent Length Scale (m)	0.001

In addition to validating the numerical results against experimental data for forces and wake survey, we also present characteristics of the flow linked to the current case study, in terms of unsteady viscous and separated flow, investigation of the laminar-turbulent transition and observation of junction flow around intersections between the components of the keel. The commercial CFD codes ANSYS FLUENT 12.1 and STAR-CCM+ v7.02 are used in the study.

3 MATHEMATICAL MODEL

3.1 LARGE EDDY SIMULATION

Large Eddy Simulation possesses good application prospect in research of flow fluctuation for its advantages in capturing instantaneous flow characteristics and unsteadiness compared to unsteady RANS. Using LES to study the instantaneous flow characteristics in engineering becomes more and more widespread, and continues to progress in reaching a level of maturity with the help in computational power increase.

3.1.1 Governing Equations

The governing equations employed for LES are obtained by filtering the time-dependent Navier-Stokes equations and the continuity equation. The filtering process effectively filters out the eddies whose scales are smaller than the filter width or grid spacing used in the computations. The resulting equations thus govern the dynamics of large eddies.

A filtered variable (denoted by an overbar) is defined by

$$\overline{\Phi}(x) = \int_D \Phi(x')G(x,x')dx' \tag{1}$$

D is the fluid domain and G is the filter function that determines the scale of the resolved eddies. Filtering the equations in incompressible form, we obtain the following formulation:

$$\frac{\partial}{\partial x_i}(\overline{u}_i) = 0 \tag{2}$$

and

$$\frac{\partial \overline{u}_i}{\partial t} + \frac{\partial}{\partial x_j}(\overline{u}_i \overline{u}_j) = -\frac{1}{\rho}\frac{\partial \overline{p}}{\partial x_i} +$$
$$\frac{\partial}{\partial x_j}\left[\nu(\frac{\partial \overline{u}_i}{\partial x_j} + \frac{\partial \overline{u}_j}{\partial x_i})\right] - \frac{\partial \tau_{ij}}{\partial x_j} + S_i \tag{3}$$

where the overbar represents the spatial filtering, called the grid-scale filter. $\overline{u}$ are the resolved velocity components, $\overline{p}$ is the resolved pressure, ρ is the density, ν is the kinematic viscosity, S_i is the source term and τ_{ij} is the subgrid-scale (SGS) stress tensor defined as:

$$\tau_{ij} = \overline{u_i u_j} - \overline{u}_i \overline{u}_j \tag{4}$$

Compared with the original Navier-Stokes governing equations, LES formulation has an additional SGS stress tensor τ_{ij}. It is a second-order symmetric tensor, which includes six independent variables, and requires modelling with different SGS models.

3.1.2 Subgrid-Scale Modelling

The subgrid-scale stresses resulting from the filtering operation are unknown, and require modelling. The SGS turbulence models employ the Boussinesq hypothesis (or eddy-viscosity assumption) as in the RANS models, computing subgrid-scale turbulent stresses from:

$$\tau_{ij} - \frac{1}{3}\tau_{kk}\delta_{ij} = -2\nu_t \overline{S}_{ij} \tag{5}$$

here ν_t is the SGS subgrid-scale stress turbulent viscosity, τ_{kk} is the isotropic part of the subgrid-scale stresses added to the filtered static pressure term. $\overline{S}_{ij}$ is the resolved strain rate tensor defined by:

$$\overline{S}_{ij} = \frac{1}{2}(\frac{\partial \overline{u}_i}{\partial x_j} + \frac{\partial \overline{u}_j}{\partial x_i}) \tag{6}$$

In the Smagorinsky-Lilly model [7], the form of the SGS eddy-viscosity is modelled by

$$\nu_t = (C_S \Delta)^2 \left| \overline{S} \right| \tag{7}$$

with $\left| \overline{S} \right| \equiv \sqrt{2 \overline{S}_{ij} \overline{S}_{ij}}$ defined as the magnitude of the resolved strain rate tensor, Δ is the filter length scale and C_S is the non-dimensional Smagorinsky constant, which is taken equal to 0.1.

In the Dynamic Smagorinsky-Lilly model, the constant C_S is calculated dynamically at every time and position in the flow based on the Germano identity and the scale invariance assumption [8, 9]. The new filter width is equal to twice the grid filter width Δ. The dynamic procedure thus obviates the need for users to specify the model constant C_S in advance.

The Germano identity is defined as:

$$L_{ij} = T_{ij} - \tilde{\tau}_{ij} \tag{8}$$

where T_{ij} is the stress at a test filter scale $\tilde{\Delta}$, and L_{ij} is the resolved stress tensor which can be computed by the resolved scales.

Applying SM to model the SGS stress at a test filter scale, T_{ij} can be expressed by:

$$T_{ij} - \frac{1}{3} T_{kk} \delta_{ij} = 2 [C_S(\tilde{\Delta}) \tilde{\Delta}]^2 \left| \tilde{S} \right| \tilde{S}_{ij} \tag{9}$$

Substituting (9) and (5) into (7), and considering the scale invariance assumption, we obtain:

$$L_{ij} - \frac{1}{3} L_{kk} \delta_{ij} = 2 (C_S \tilde{\Delta})^2 \left| \tilde{S} \right| \tilde{S}_{ij} - 2 (C_S \Delta)^2 \left| \hat{\overline{S}} \right| \hat{\overline{S}}_{ij} \tag{10}$$

Assuming $M_{ij} = 2 \tilde{\Delta}^2 \left| \tilde{S} \right| \tilde{S}_{ij} - 2 \Delta^2 \left| \hat{\overline{S}} \right| \hat{\overline{S}}_{ij}$, (10) can be rewritten as:

$$C_S = \frac{L_{ij} - \frac{1}{3} \delta_{ij} L_{kk}}{M_{ij} M_{ij}} \tag{11}$$

The C_S obtained using the dynamic Smagorinsky-Lilly model varies in time and space over a wide range. To avoid numerical instabilities, its value is clipped between zero and 0.23. The upper bound limit aims at preventing the appearance of high C_S values that, on one hand, are not physical and on the other can lead to high spatial variations of Cs and destabilize the solver.

Finally, the third SGS model of interest is the Wall-Adapting Local Eddy-Viscosity model (WALE) of Nicoud and Ducros [10]. The WALE model is a Smagorinsky type model but with a modified dependence on the resolved strain field, which is supposed to provide improved near-wall behaviour. The difference with the previous models comes in the way the eddy viscosity is modelled (7):

$$\nu_t = (C_w \Delta)^2 \frac{(S_{ij}^d S_{ij}^d)^{3/2}}{(\overline{S}_{ij} \overline{S}_{ij})^{5/2} + (S_{ij}^d S_{ij}^d)^{5/4}} \tag{12}$$

where S_{ij}^d is a deviatoric part of rate-of-strain tensor.

The default value of the WALE constant, C_w is 0.325 and has been found to yield satisfactory results for a wide range of flow. The rest of the notation is the same as for the Smagorinsky-Lilly model.

3.2 DETACHED EDDY SIMULATION

In the DES method, the unsteady RANS models are employed in the near-wall regions, while the filtered versions of the same models are used in the regions away from the near-wall. The LES region is normally associated with the core turbulent region where large turbulence scales play a dominant role. In this region, the DES models recover the respective subgrid models. In the near-wall region, the respective RANS models are recovered.

3.2.1 Realizable κ-ε Model

This RANS model is similar to the well known realizable κ-ε model [11] with the exception of the dissipation term in the κ equation. In the DES model, the Realizable κ-ε RANS dissipation term is modified such that:

$$Y_\kappa = \frac{\rho \kappa^{3/2}}{l_{des}} \tag{13}$$

where:

$$l_{des} = \min(l_{r\kappa e}, l_{les}) \tag{12}$$

$$l_{rke} = \frac{k^{3/2}}{\varepsilon} \tag{13}$$

$$l_{les} = C_{des} \Delta \tag{14}$$

C_{des} is a calibration constant used in the DES model and has a value of 0.61 and Δ is the maximum local grid spacing in x-, y- z- direction.

3.2.2 SST κ-ω Model

The dissipation term of the turbulent kinetic energy from the standard κ-ω model [12] is modified for the DES turbulence model as described by Menter [13] such that:

$$Y_\kappa = \rho \beta^* \kappa \omega F_{DES} \tag{15}$$

where $F_{DES} = \max(\dfrac{L_t}{C_{des}\Delta}, 1)$, with C_{des} and Δ as

above, and $L_t = \dfrac{\sqrt{\kappa}}{\beta^*\omega}$.

STAR-CCM+ employs the following SGS models: SM and WALE for LES and SST κ-ω for DES. ANSYS FLUENT also offers the Dynamic Smagorinsky-Lilly and the Realizable κ-ε. In the present study, the different models are used and compared between the two solvers.

4. COMPUTATIONAL AND NUMERICAL APPROACH

4.1 COMPUTATIONAL DOMAIN AND MESH

The computational domain was reproduced as an exact copy of the experimental set-up; therefore, it is identified as a 'virtual wind tunnel'. The complete test section was modelled from the inlet plane, where the wind tunnel contraction ends, to the outlet plane, where the expansion begins. The domain dimensions are Length (m) x Width (m) x Height (m): 2.5 x 1.8 x 1.25. The coordinate system was defined at the inlet base of the tunnel, x-direction streamwise, y-direction upwards and z-direction transversally. As mentioned previously, blockage effects were neglected as they are not influencing the outcome of the simulation results.

Two types of mesh were created for the purpose of the study. On one hand, the simulations were performed on a single-block adapted unstructured mesh consisting of prismatic cells in the boundary layer and vicinity of the keel, with tetrahedral cells in the outer part of the volume. Surface mesh on the keel comprised on triangular face elements. This type of grid was associated with the ANSYS FLUENT simulations and developed following the lessons learned and the finding of previous study [6]. A view of the mesh can be seen in Figure 2. The adapted unstructured approach is the most suitable for this solver, because of the complexity of the geometry and the flexibility it offers to the user.
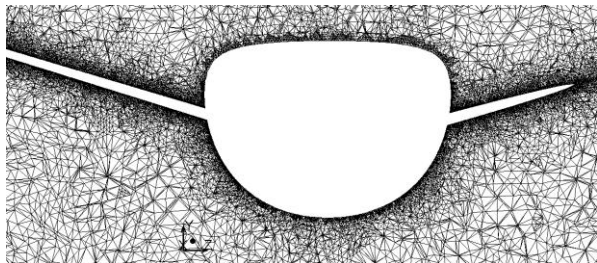

Figure 2: plane cut of mesh around the winglets, unstructured grid, ANSYS FLUENT

On the other hand, the automated meshing approach offered by STAR-CCM+ was used. The meshes employed were predominantly hexahedral trimmed non-structured grids incorporating a prism layer mesh around the keel and were generated in STAR-CCM+. The grids were based upon the medium-to-fine density (base size between 10-20) size control with additional anisotropic volumetric refinement in the relevant areas where the flow is expected to be important (boundary layer, wake, separated areas, winglets). This approach allows the grid resolution to be increased in the turbulent wake pattern region only around the keel if necessary.
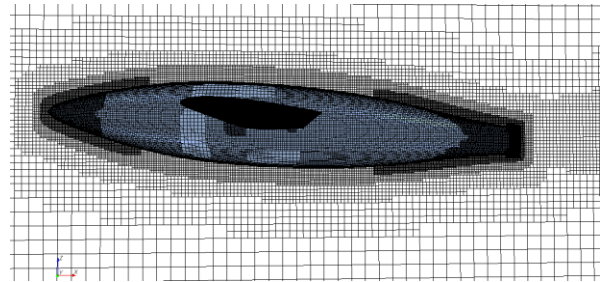

Figure 3: Computational domain, trimmed cells, meshed with STAR-CCM+

The near-wall boundary layers were extruded at a rate of 1.1 from the surface of the model, and depending on the configuration, comprised of between 5 and 20 inflation layers in total. The first cell height was kept to a minimum, of the order of 1-10 μm, resulting in a y^+ value of under 5. For the coarsest meshes, this value was increased and wall-function treatments were used near the model (in DES). The grid spacing, normalised by friction velocity and viscosity, at the wall was $(\Delta x^+; \Delta y^+; \Delta z^+) \approx (30\text{-}80; 1\text{-}5; 20)$ for unstructured mesh and $(\Delta x^+; \Delta y^+; \Delta z^+) \approx (12\text{-}110; 0.3\text{-}1; 15)$ for the cut-cell mesh.

The simulation grids consisted of between 3 to 8 million elements. This resolution was reached based on the mesh specifications defined (near-wall resolution, refinement in specific areas …), the experience from previous study [6] and using the computational resources available for handling such large mesh sizes.

4.2 BOUNDARY CONDITIONS

A constant velocity condition of 36.27 m/s with 0.1% turbulence intensity was applied as a boundary condition at the inlet of the domain. They correspond to the values used in the experiments and defined in Table 2. At the outlet of the domain, zero static pressure is imposed. On the surface of the appendage, no-slip condition was employed. To ease computational time, the tunnel walls were defined as slipped surfaces.

Since LES and DES are unsteady models, the velocity profile imposed at the inlet of the domain must be time-dependent. To model the fluctuating velocity, several techniques exist to account for this. In the study, the Vortex Method was employed for both solvers [15, 16].

It consists of generating and transporting randomly in the inlet plane a given number (in this study 190) of 2D vortices whose intensity and size depend on the local value of κ, the turbulence dissipation rate or the turbulent intensity, for which profiles are prescribed based on the experiment. The advantage of this method is that it does not require additional simulation.

4.3 NUMERICAL SOLUTION

An implicit, segregated solver was chosen as the solver algorithm. Second-order temporal discretization was used. The bounded central-differencing scheme is used to discretize the convection term in the filtered momentum equation in FLUENT. In STAR-CCM+, the pure central-differencing scheme is adopted. The flow velocities and pressures in the domain are calculated using the standard SIMPLE (STAR-CCM+) or SIMPLEC (FLUENT) pressure correction method. A second-order upwind differencing scheme was employed for the solution of the momentum and turbulence equations. An algebraic multigrid method is employed to accelerate solution convergence.

The steady state computation was initially carried out with the solution of a preceding RANS calculation to have a convergence below $10^{-3}/10^{-4}$ depending on the case (forces, residuals, surface values were monitored). After, the unsteady simulation to model the fluctuating velocity is superimposed. The time-step value has been adapted for the computational grids (between $10^{-4}-10^{-6}$ seconds of order of magnitude). One flow-through time was equivalent to about 0.069s ($T_{ft}=L/U_\infty$, where L is the domain's length). LES and DES were run for a sufficiently long flow-time to obtain stable statistic of flow and turbulence ($35-45T_{ft}$), and further to gather relevant data for the results ($45T_{ft}$). Simulation were performed on an Intel Xeon 2 CPUs with eight cores, 24 GB Ram capacity and of processing power equal to 3.2 GHz. The computations were run in parallel processing.

5 RESULTS AND DISCUSSION

In this section, a selection of results will be presented and discussed, based on the CFD simulations performed for this study. The validation consisted of comparing the global loads on the keel, and the prediction of the velocity magnitude for the wake survey. Other results presented are relevant examples of the flow encountered in keel hydrodynamics and of the capabilities of LES and DES to capture the complexity of the flow.

5.1 GLOBAL FORCES ON KEEL

The results obtained from the present CFD calculations are compared to the experimental values of Werner in terms of time-averaged Lift (L) and drag (D) forces. The later is measured longitudinally in the direction of

the undisturbed flow and the former is taken perpendicular to the wind, along the z-axis.

The exp uncertainty of the forces was 3.2% for the lift and 3.1% for the drag and is shown in the graphs in the form of error bars. For clarity sake, the figures have been refined near the measured force values, so that the differences between the turbulence models and the CFD solvers can be appreciated. Results shown here are for grids of around 3.5 million cells for the no wings configuration, and about 6 million for the winglets in forward position.
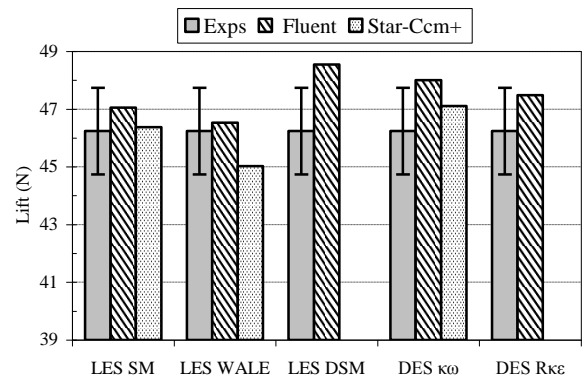

Figure 4a: Comparison of lift force for CFD models, no-wing configuration
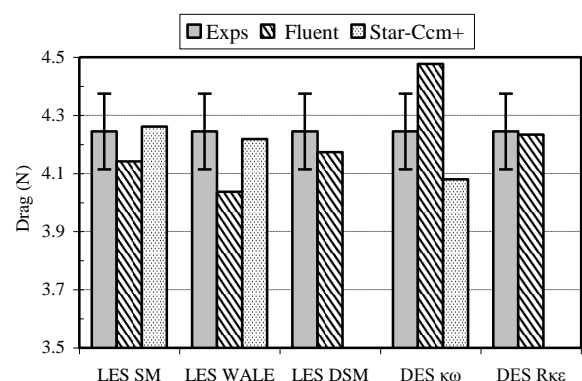

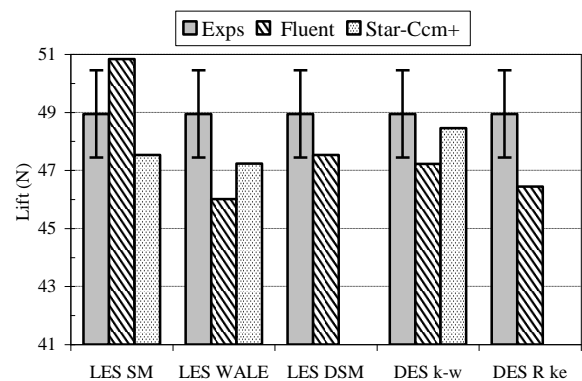Figure 4b: Comparison of drag force for CFD models, no-wing configuration

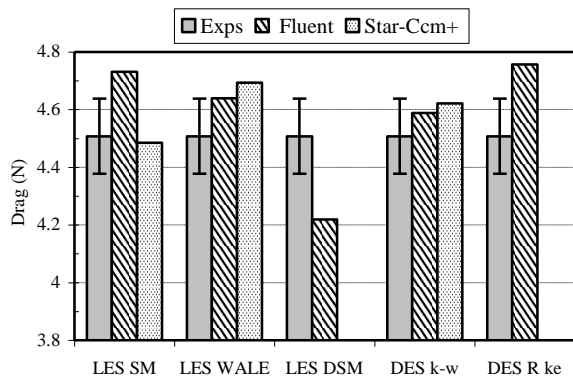Figure 5a: Comparison of lift force for CFD models, forward wings configuration

Figure 5b: Comparison of drag force for CFD models, forward wings configuration

The results are in quite a good agreement with the experimental data and represent a much-improved performance compared to the previous data published with one of the numerical solver by the author [6], for both cases with and without winglets. Most of the turbulence models for both solvers are within the experimental uncertainty.

Comparing case by case, STAR-CCM+ gives the most accurate results in the non-winged keel computations. The main differences are found for the drag prediction of the DES κω model, likely linked to the fact that a Delayed DES model was chosen in the simulation. The results with Fluent show a wider range of estimations depending on the model. The highest errors were found to be about 5.6%.

For the forces computed in the other configuration, the discrepancies in the models are slightly larger than the previous case. The flow is more complex but the results are still within a range of validity. Again STAR-CCM+ outperforms Fluent on all common models, baring the drag prediction of the WALE model, where it is above the experimental uncertainty and above fluent.

Differences in the two codes are likely down to the different mesh topology, since numerical formulation was almost identical for both codes; non-structured hexahedral trimmed cells look to be more accurate than the tetrahedral unstructured cells of the other solver. A thorough error and uncertainty analysis is required in the future though, particularly for advanced numerical models.

5.2 WAKE SURVEY

To assess the accuracy of the methods in terms of velocity and vortex structure at the far field, a comparison of the wake at a given plane behind the keel has been carried. Results for the case without wings are presented. This type of assessment is instructive in cases when data such as surface pressure, velocity measurements on or near the body are not

obtained from experiments. As the two solvers use different grid topology, observing the wake of the flow is important in evaluating the CFD simulations in terms of level of accuracy and turbulence models. The velocity magnitude was measured in a wake plane orthogonal to the undisturbed flow defined at x/L: 0.95 from the wind tunnel inlet. Numerical results are shown for grids of around 3.5 million cells.

Figure 6 shows the comparison of the velocity magnitude contours for DES SST κω (averaged values) & for LES SM (instantaneous values taken at $t = 2s$) in the turbulent wake. Areas of low velocity correspond to regions of high vorticity magnitude. Three main vortices can be identified [3]; they are in the clockwise direction (view is looking downstream, leeward side to the right) from top to bottom: the bulb-tip vortex, the bilge vortex and the fin junction vortex.

The overall wake shape and position is in fair agreement with the experimental data. Vortex shape and intensity in the bulb wake can be considered satisfactory; there is some lack of resolution in the bottom part of the vortex for most but the overall trend is reasonable.

The DES predictions of Star-CCM+ are in satisfactory agreement with the tunnel measurements. The velocity is slightly underpredicted as are the bilge and the junction vortices. General trend is good. If we link to the force results, then we can observe that refinement is needed in the longitudinal to resolve the vortices better (drag is under predicted). The results from Fluent results differ in magnitude and resolution of the vortices, and not corresponding to the higher value of drag reported in the force comparison.

The instantaneous velocity contours show the unsteady nature of the flow in the wake, exhibiting a number of additional vortices on top of those reported. Depending on the grid topology, vortices are more developed, but main contours appear to be in the correct location. The range in Velocity magnitude is slightly underpredicted by both solvers, but within an acceptable range of validity and in agreement with the forces prediction.

It can be seen from the results that κω SST is recommendable for both solvers and mesh type, with preference to hexahedral trimmed cells. Performance is matching that of experiments. For that specific case, the cell size in the wake region was too coarse. Prediction was found to be increasing in details with targeted refinement and cell size control. Another possible explanation may the Vortex Method set at the inlet boundary and the turbulent intensity, which seem to work better in one of the solvers.
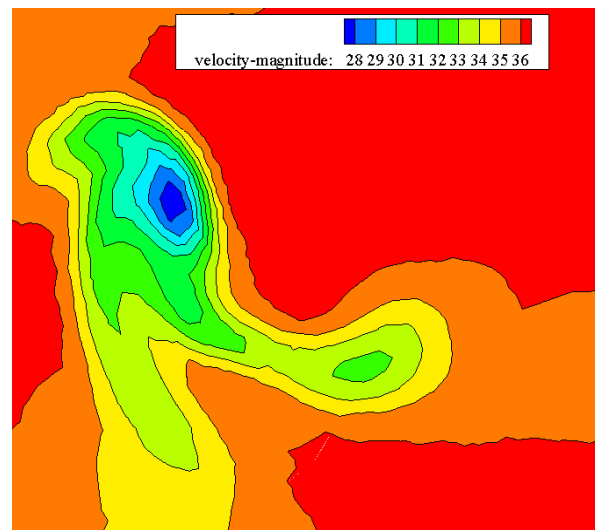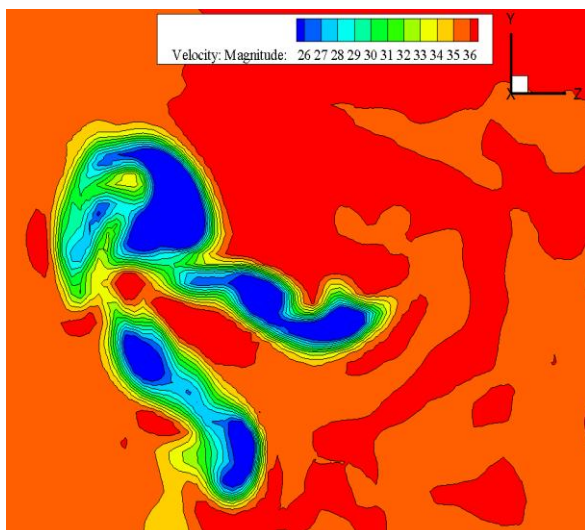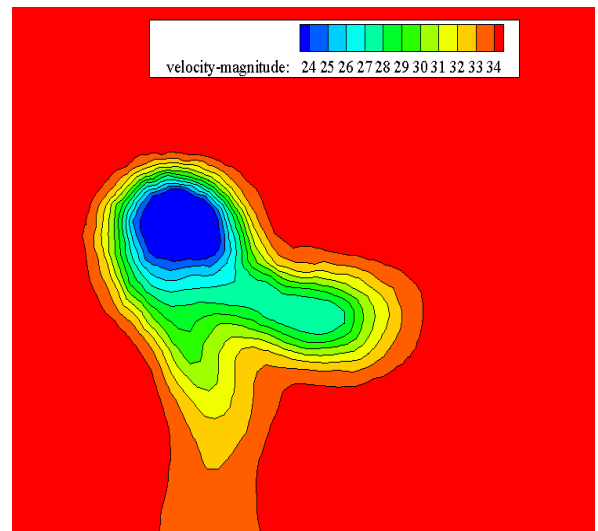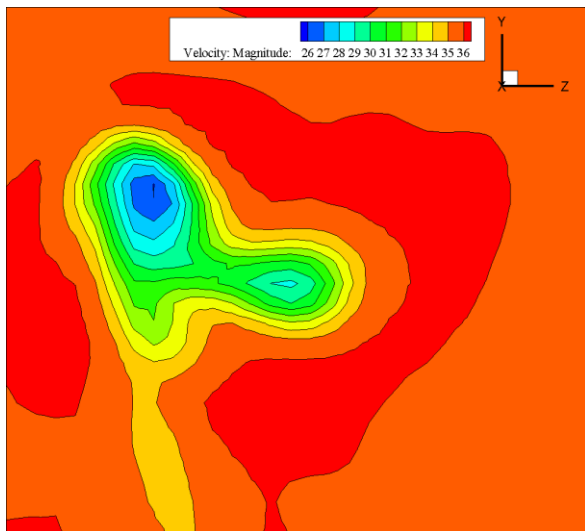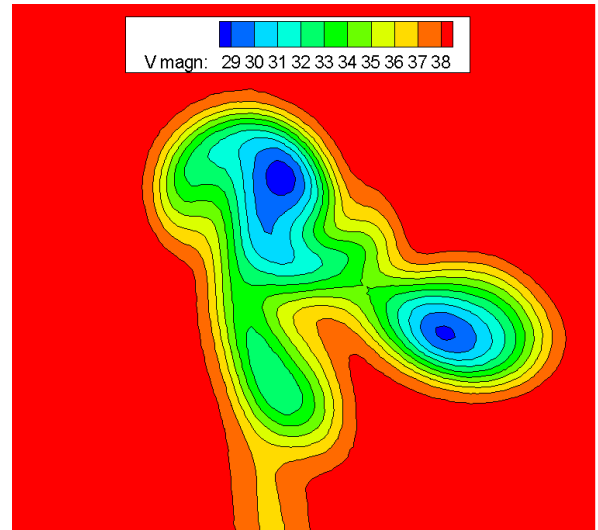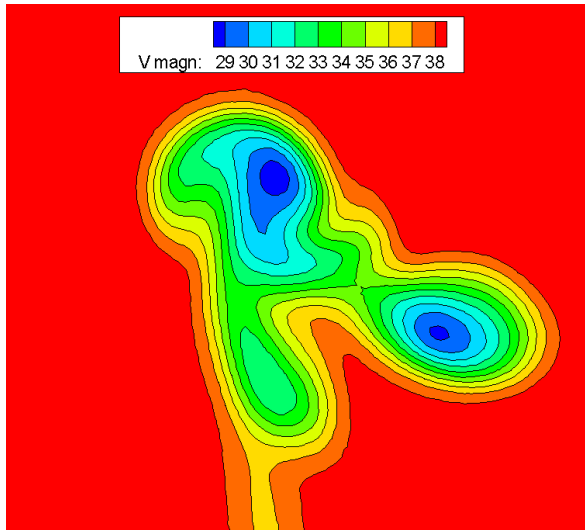
Figure 6a: Contours of velocity magnitude at wake plane with STAR-CCM+. Top to bottom: Experiments, DES κω SST and LES SM models

Figure 6b: Contours of velocity magnitude at wake plane with ANSYS Fluent. Top to bottom: Experiments, DES κω SST and LES SM models

5.3 UNSTEADY FLOW REGIME

5.3.1 Vortices and junction flow

Flow past an appended keel is a challenging case for CFD because of the different flow regimes around the body; including the laminar boundary layer, transition region, turbulent boundary layer, separation point, and separation region as well as wake region. There were no other formal observations during the experiments of the flow to report as comparison, but physics of the flow can be reported.

At the yaw angle of the measurements, separation is expected to occur at the trailing edge of the suction side of the model. Although it can be argued that there is no massive separation to justify the use of LES or DES (i.e. large angles of attack), the models nonetheless predict the flow unsteadiness in a characteristic manner. LES is particularly suitable to investigate the generation and evolution of coherent structures in turbulent flows. Figure 7 shows the instantaneous flow pathlines at the intersection close of the fin with the bulb. The vortical structures emanate from the junction towards the end of the trailing edge and from the bulb. The rotation in the flow carries on further down the length of the bulb and in the wake; these vortices, move towards the starboard side, as expected.
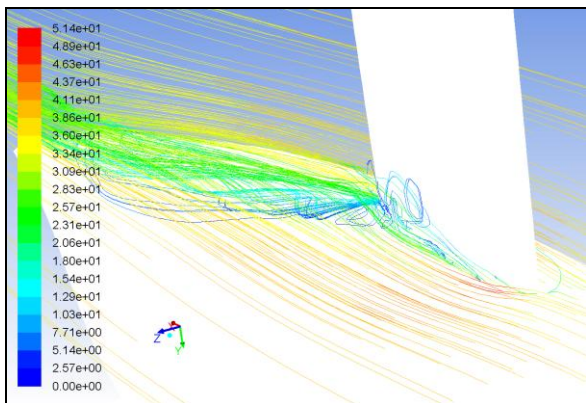

Figure 7: Pathlines coloured by velocity magnitude near the fin/bulb junction

Similarly, the surface streamlines on the keel show the presence of a horseshoe vortex when the undisturbed flow reaches the fin at the junction with the bulb; figure 8. On the trailing edge, reattachment occurs. The flow remains unsteady and turbulent in the aft part, inducing further separation down the keel. In the pressure side, the flow is less disturbed, due to the yaw angle, pressure transfers from the windward to the leeward side. The surface streamlines show that the numerical simulations capture the important features of the recirculation zone. Similar behaviour is reported for the flow near the winglets, but not as pronounced because the winglets pitch was zero degrees. In terms of code comparison, both solvers predict the vortices and the separation and recirculation on the body.
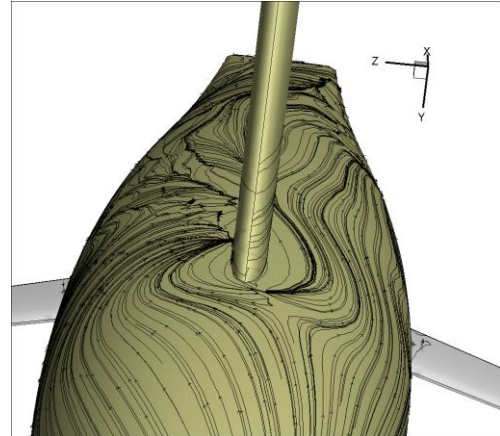

Figure 8: Surface streamlines on the appended keel.

5.3.2 Laminar and turbulent flow

Turbulence is expected around the fin and the winglets over most part of the structures. Based on the inlet flow, their Reynolds number is equal to $Re_f = 5.04 \times 10^5$ and $Re_w = 1.80 \times 10^5$ respectively, which means transition will occur sooner than for the bulb. In computational terms, this means that further resolution may be necessary near the wall of these lifting surfaces to fully grasp the unsteadiness and the transition from laminar to turbulent flow. The flow around the bulb is laminar over a longer part, whereas the turbulence on the fin and the winglets is much more pronounced.

As an example, figures 9 and 10 show the instantaneous velocity vectors in the boundary layer of the fin at the plane y = 0.61, over a part of the cross section near the intersection with the bulb. The top picture shows the trailing edge on the leeward side, and the bottom is the leading edge on the windward side. A vortex structure can be identified on the trailing edge, with separation and turbulence occurring on the viscous sublayer. The flow then reattaches after the vortex. On the pressure side, there is less relevant turbulent effect and the flow exhibits a laminar regime over a longer range. It appears more energized; as a result, the boundary layer thickness in the pressure side is much thinner than in the suction side. The regions of stagnation points, reattachment and separation on the suction side correspond to changes in the surface pressure of the fin, due to the flow unsteadiness.

The streamlines show that the numerical solution captures the important features of the boundary layer including separation, recirculation zone and turbulent boundary layer. Further insight into these complex phenomena is required, with the investigation of parameters influencing the turbulence for LES and DES, such as intensity and turbulent viscosity at the inlet.
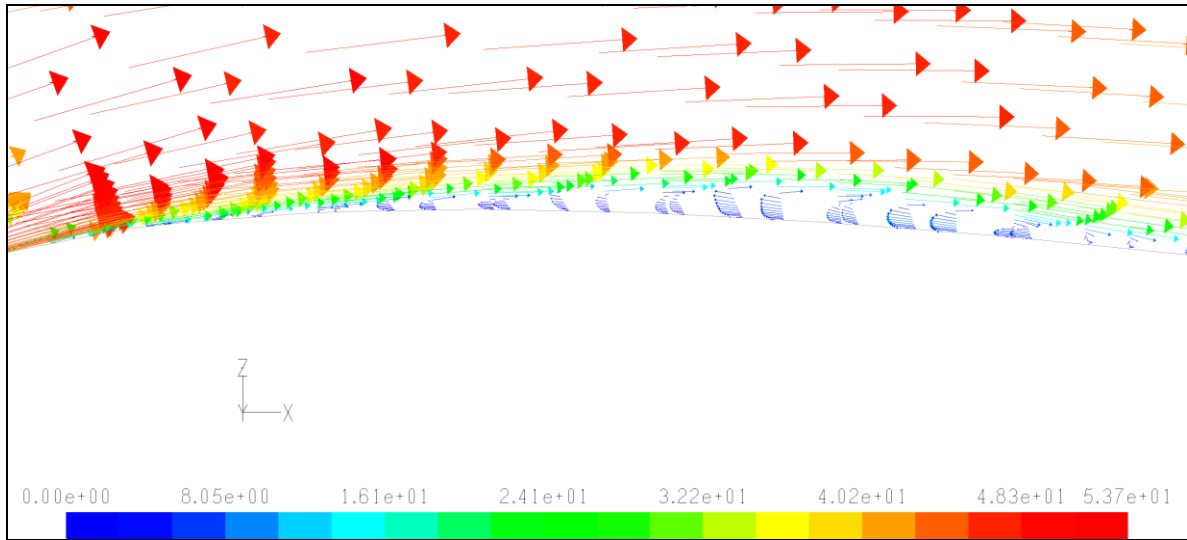
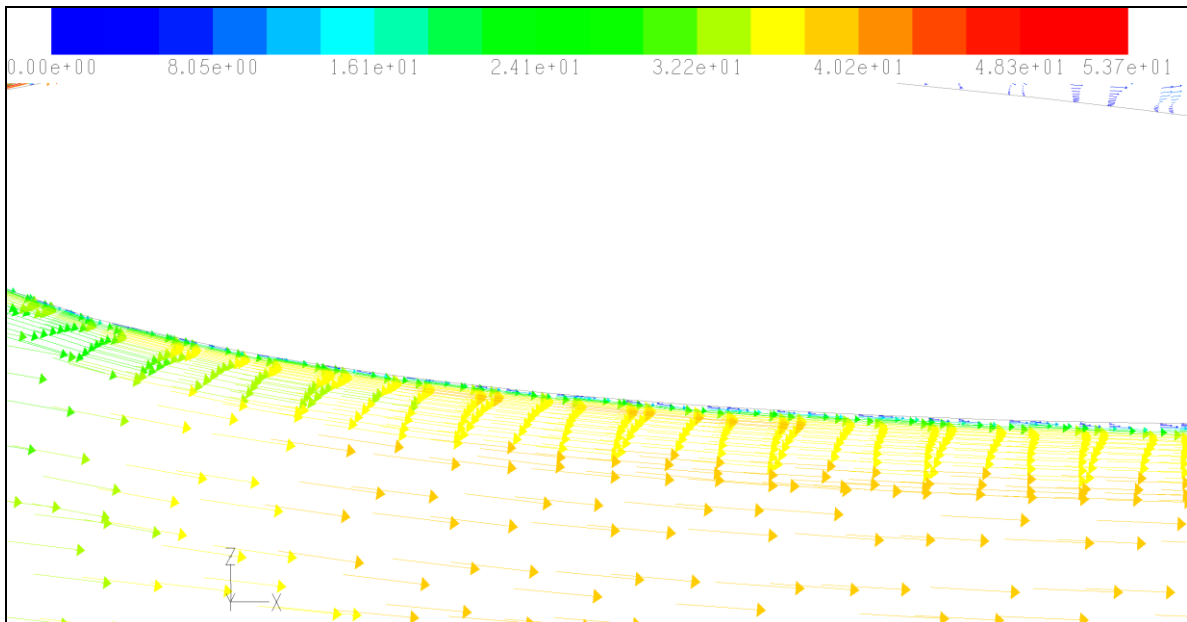Figure 9: Velocity vectors in the boundary layer, on the leeward side (TE)

Figure 10: Velocity vectors in the boundary layer, on the windward side (LE)

6 CONCLUSIONS

In the present paper the hydrodynamic performance of and asymmetric keel at yaw angle is presented using advanced CFD based on the Large Eddy Simulation and Detached Eddy Simulation turbulence models. Two solvers were tested, with two different grid types. Results obtained were compared quantitatively against wind-tunnel forces and wake plane observation.

The following observations and conclusions can be drawn from the results obtained in the current study:

- The forces prediction showed a significant improvement compared to previous study, with a maximum error of about 6%.

- The hexahedral non-structured grid offered a better prediction of forces and a more detailed account of the wake flow than tetrahedral unstructured mesh
- Characteristics of the flow such as separation, vortices, and wakes are correctly predicted and resolved qualitatively.
- Likely influence of some inlet parameters depending on the grid topology, the SGS model and the solver.

Possible directions of future research and developments in this research topic will consist of the following:

- Introduce the laminar zones around part of the bulb and fin keel

- Investigate the transition models of the solvers further.
- Study the influence of winglets' pitch angles, likely to influence the separation and exhibit flow features
- Apply the cut cell method of ANSYS FLUENT 13.0 to compare with equivalent method used by STAR-CCM+.
- Investigate uncertainty and errors of CFD
- Modify and use different inlet boundary conditions (Spectral Synthesizer, turbulent intensity, viscosity ratio)

ACKNOWLEDGEMENTS

REFERENCES

1. TINOCO, E. N., GENTRY, A. E., BOGATAJ, P., SEVIGNY, E. G., and CHANCE, B., 'IACC Appendage Studies', *Proceedings of the 11th Chesapeake Sailing Yacht Symposium,* 1993.

2. WERNER, S., LARSSON, L., and REGNSTROM, B., 'A CFD Validation Test Case - Wind Tunnel Tests of a Winglet Keel', *2nd High Performance Yacht Design Conference,* 2006.

3. WERNER, S., PISTIDDA, A., LARSSON, L., REGNSTROM, B., 'Computational Fluid Dynamics Validation for a Fin/Bulb/Winglet Keel Configuration', *Journal of Ship Research, Vol. 51, No. 4,* 2007.

4. AMBROGI, M.M., BROGLIA, R., DI MASCIO, A., 'Numerical Simulation of a flow around an America's Cup Class Keel', *Proceedings of the 18th International Offshore and Polar Engineering Conference,* 2008.

5. THYS, M., 'Performance Evaluation of a Sailing Yacht with the Potential Code RAPID', *ENSTA,* France, 2008.

6. MYLONAS, D., and SAYER, P., 'The hydrodynamic flow around a yacht keel based on LES and DES', *Ocean Engineering 46: 18-32,* 2012.

7. SMAGORINSKY, J., 'General Circulation Experiments with the Primitive Equations. I the Basic Experiment', *Monthly Weather Review, vol. 91, 99-164,* 1963.

8. GERMANO, M., PIOMELLI, U., MOIN, P., and CABOT, W.H., 'Dynamic Subgrid-Scale Eddy Viscosity Model', *Summer Workshop, Center for Turbulence Research, Stanford, CA,* 1996.

9. LILLY, D.K., 'A Proposed Modification of the Germano Subgrid-Scale Closure Model', *Physics of Fluids, 4:633-635,* 1992.

10. NICOUD, F., and DUCROS, F., 'Subgrid-scale modelling based on the square of the velocity gradient tensor', *Flow, Turbulence and Combustion, vol. 62, pp-183-200,* 1999.

11. SHIH, T. H., et al. 'A new κ-ε eddy viscosity model for high Reynolds number turbulent flows', *Computers & Fluids 24 (3): 227-238,* 1995.

12. WILCOX, D. C., 'Turbulence Modeling for CFD', *DCW Industries, Inc.,* 1998.

13. MENTER, F.R., KUNTZ, M., and LANGTRY, R., 'Ten Years of Experience with the SST Turbulence Model', *Turbulence, Heat and Mass Transfer 4, pages 625-632,* 2003

14 ANSYS FLUENT, 'Fluent 12.1 User Manual', *ANSYS Inc,* 2009.

15 SERGENT, E., 'Vers une méthodologie de couplage entre la Simulation des Grandes Echelles et les modèles statistiques.', PhD thesis, *L'Ecole Centrale de Lyon,* 2002.

16 MATHEY, F., COKLJAT, D., BERTOGLIO, J. P., SERGENT, E., 'Assessment of the vortex method for large eddy simulation inlet conditions', *Progress in Computational Fluid Dynamics, An International Journal,* 6(1), 58-67, 2006.

17 CD-ADAPCO, 'STAR-CCM+ 6.02.007 User Guide', *CD-Adapco,* 2011.

AUTHORS BIOGRAPHY

D. Mylonas has recently completed his PhD in the Department of Naval Architecture and Marine Engineering, University of Strathclyde, Glasgow and officially graduates in July 2013. His research topic focused on the application of LES and DES in yacht hydrodynamics. He also holds an M.Eng from the same department. Other interests include ship & marine hydrodynamics, smart materials, yacht design and CFD simulations on marine and aerodynamic applications.

S. Turkmen is a PhD student in the Department of Naval Architecture and Marine Engineering, University of Strathclyde, Glasgow. He has been researching on the topic of smart material application to mitigate noise and vibration in ships. He is also investigating underwater-radiated noise due to the cavitating propellers.

M. Khorasanchi is a research fellow in the Department of Naval Architecture and Marine Engineering, University of Strathclyde, Glasgow. Dr Khorasanchi has carried out several studies on vortex-induced-vibration (VIV) of marine risers and VIV suppression devices. His current teaching and research interests centre on hydrodynamics and marine propulsion. He investigates the hydrodynamic performance of marine vessels through full-scale CFD simulation. He also works on retrofitting technologies to improve the performance of marine vessels and reduce the fuel consumption and carbon emission of shipping industry.